forumacusticum 2023

LASER SHOCK WAVE PROPAGATION IN A 3D WOVEN COMPOSITE MATERIAL : EXPERIMENT AND SIMULATION

Eduardo Cuenca, Mathieu Ducousso
Safran Tech
Magny les Hameaux
France
mathieu.ducousso
@safrangroup.com

Laurent Berthe
PIMM, CNRS
& Arts et Métiers Paris Tech
Paris, France
laurent.berthe
@cnrs.fr

François Coulouvrat
∂'Alembert, CNRS
& Sorbonne Université
Paris, France
francois.coulouvrat
@sorbonne-universite.fr

ABSTRACT

The propagation of a laser shock wave within a composite material used in aeronautics is investigated. The material is made of carbon fibres woven according to a 3D pattern within an epoxy matrix. A shock wave is generated by an impulsive (of order 10 ns) intense laser beam of power a few GW/cm^2, focused on the surface of a thin metallic layer attached to the composite. The metallic surface ablation results in an expanding plasma inducing a shock wave in the material with a peak stress of a few GPa. Its propagation can be measured by the velocity of the opposite surface of the sample detected by laser interferometry. The high frequency content of the signal and the heterogeneous and anisotropic behaviour of the material induce a complex propagation. A measurement campaign has been performed for different samples. A 2D numerical model has been developed based on a finite difference discretisation of the equations of linear elastodynamics for the propagation part, combined with a nonlinear model of the source. Sample geometry and fibre orientations are obtained from analysis of the images of transversal cuts of the samples. Experimental data are statistically compared to the model and discussed.

Keywords: *shock waves, laser, composite material, FDTD numerical simulation*

1. INTRODUCTION

Reduction of CO_2 and other greenhouse gases emissions is one of the major challenges of the aeronautical transport sector. One of the most efficient ways for this alleviation is to replace metallic parts of the structure by composite materials. Safran, in its new LEAP engine (manufactured by CFM International, a 50/50 joint venture between Safran and General Electric) use fan blades made of matrix composite materials, with only a titanium leading edge attached to each of them. The fan carter is also made of this same material. The total weight saving of the LEAP engine compared to the CFM56 is 454 kg per aircraft. This fan weight reduction allows to enlarge the engine diameter, increase the engine by-pass-ratio and reduce noise emissions. The LEAP engine is able to decrease the fuel consumption, and therefore its CO_2 emissions, by 15% compared to previous generation engines, while also reducing NO_x emissions by 50% and satisfying ICAO's Chapter 14 most stringent noise standards.

2. DESCRIPTION OF MATERIAL

The Tisse3D material is the 3D woven-composite material designed, developed and produced by Safran Group, in partnership with the American company Albany International, to constitute the fan blades of its LEAP engine. Three-dimensional weaving process allows to produce complex woven reinforcements with (i) reduced weight compared to metallic materials, (ii) enhanced mechanical properties compared to classical composites, especially resistance to delamination and impact in the three directions of space, and (iii) adaptation to the desired shape of the product. Figure 1 (top) is a photography (with microscope Axio Observer (Zeiss) using RGB mode with a 2.5x zoom) of the cross-section of the Tisse3D obtained after cutting the sample with a microtome SECOTOM-50 cutting machine and polishing the surface. Scales are not indicated for reasons of industrial confidentiality.
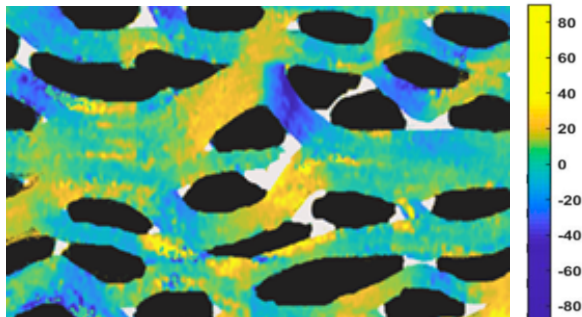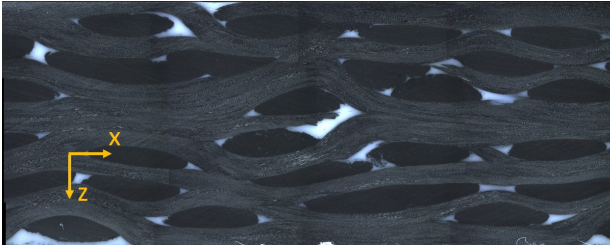
Figure 1. Top: photography of one cross-section. The white structure corresponds to the epoxy resin. Carbon fibre reinforcement appears either in gray (in-plane fibres) or in black (transverse fibres). Bottom : example of colour map of the local orientation angle with respect to the horizontal direction, in degrees. Epoxy in white and tows of micrometric fibres transverse to the plane in black.

Two different components can be distinguished. The darkest one is for the tows of carbon PolyAcrylonitrile (PAN)-based microfibres manufactured by Hexcel, of diameter around 5 μm. These tows are intertwined between one another to conform the 3D reinforcement structure of the composite. The white material of the image is the poly-epoxide resin (manufactured by Solvia). The resin fills the voids of the Tisse3D reinforcement, but also the space between the microfibres in the tows, giving integrity to the structure when cured during a couple of hours at around 180°C. The Fibre Volume Fraction (percentage ratio between carbon fibres and epoxy resin volumes) ranges between 80-20 and 90-10. In the image, two different types of tows are visible : darker ellipses are indeed tows crossing the image plane mostly perpendicularly, while

grey thick threads are tows extending mostly within the image plane. Even if tows go mainly along the horizontal axis x (for grey ones) or the transverse one y (for black ones), they also cross two or more layers of tows in the z-axis. However, an inspection of the cross-section shows samples have a quasi 2D periodic horizontal pattern that is repeated all along. Two groups of materials will be examined, the second type having a quasi-period larger than the first one. Since the shockwave investigated in this manuscript will propagate mostly through the sample thickness in the z-direction, the disposition and orientation of the tows that pack the sample will have a strong influence on the sample mechanical properties, and therefore on the wave propagation. Thus, due to its manufacturing process, each composite sample is going to be unique, strongly heterogeneous (because of the different materials used in the composite) and anisotropic (because of the manufacturing of the microfibres and of the tows themselves, and because of the woven arrangement).

Mechanical properties of both materials are reported in Tab.(1). Figures are however rounded for reasons of confidentiality, since they arise from data sheets and internal documents from Safran.

	E_l	E_t	G_{lt}	ν_{lt}	ν_t	ρ
Fibers	250	15	25	0.3	0.3	1780
Resin	5	5	1.9	0.316	0.316	1250

Table 1. Mechanical properties of the carbon fibres and of the epoxy resin. E is for Young modulus and G for shear modulus (unit: GPa), ν for Poisson ratio and ρ for density (unit: kg/m^3.). Index $_t$ is for the plane transverse to, and index $_l$ is for the fibres axial direction.

3. IMAGE ANALYSIS AND TOWS ORIENTATION

To simulate the shock wave propagation, we need to separate the tisse3D constituents numerically and determine the local orientation of in-plane tows. With this in view, we inspect the image numerically by means of Fiji (https://fiji.sc/), an open source image processing package with many bundled plugins developed initially for the analysis of biomedical images [1, 2]. From the various grey levels of each pixel within one image, we select the maximal grey range for the epoxy pixels, which appear as

the lightest ones, and the minimal one for the perpendicular tows which are the darkest ones. The intermediate values correspond to the in-plane tows. To suppress clouds of isolated light or dark points spread over most of the image, we use ImageJ plugin from Fiji to "clean" the material data by hand. To obtain the local orientation, we use within the OrientationJ plugin of Fiji, a tool called Vector Field [3] that determines the local orientation of the tows from an image in each "pack" of pixels of a user-chosen 'grid size'. For instance, if the original size of the image is 1000x100 and the chosen grid size is 10, the resulting orientation matrix is a 100x10 matrix. We therefore assume that every point within one pack has the same orientation value, thus recovering the required 1000x100 orientation matrix. Orientation is then used only for in-plane tow pixels. Fig.1 (bottom) provides the resulting colormap of the local orientation θ of the in-plane tows with respect to the horizontal axis x in degrees, while epoxy appears as white and transverse tows as black. From this rotation information, we calculate the local stiffness matrix c_{loc} knowing the material stiffness matrix. At 2D, the resulting equations of motion are

$$\frac{\partial \sigma_{xx}}{\partial t} = c_{11}\frac{\partial U}{\partial x} + c_{13}\frac{\partial V}{\partial z} + c_{15}\left(\frac{\partial U}{\partial z} + \frac{\partial V}{\partial x}\right) \quad (1)$$

$$\frac{\partial \sigma_{zz}}{\partial t} = c_{13}\frac{\partial U}{\partial x} + c_{33}\frac{\partial V}{\partial z} + c_{35}\left(\frac{\partial U}{\partial z} + \frac{\partial V}{\partial x}\right) \quad (2)$$

$$\frac{\partial \sigma_{xz}}{\partial t} = c_{55}\left(\frac{\partial U}{\partial z} + \frac{\partial V}{\partial x}\right) + c_{15}\frac{\partial U}{\partial x} + c_{35}\frac{\partial V}{\partial z} \quad (3)$$

for constitutive relations and

$$\rho\frac{\partial U}{\partial t} = \frac{\partial \sigma_{xx}}{\partial x} + \frac{\partial \sigma_{xz}}{\partial z} \quad (4)$$

$$\rho\frac{\partial V}{\partial t} = \frac{\partial \sigma_{xz}}{\partial x} + \frac{\partial \sigma_{zz}}{\partial z}. \quad (5)$$

for momentum balance, with U the material velocity in the x direction and V in the z one, and with values of density ρ and of stiffness matrix c_{loc} coefficients c_{11}, c_{13}, c_{15}, c_{35} and c_{55} varying locally with material and local orientation.

4. EXPERIMENTAL SET-UP

As sketched on Fig.2.A, an intense laser (Thales, France) emits a Nd:YAG pulse at 532 nm with a repetition frequency of 2 Hz and an energy up to 7J with a Gaussian temporal shape of duration 7 ns. The laser beam is focused by an optical lens of focal diameter 4.7 mm. A
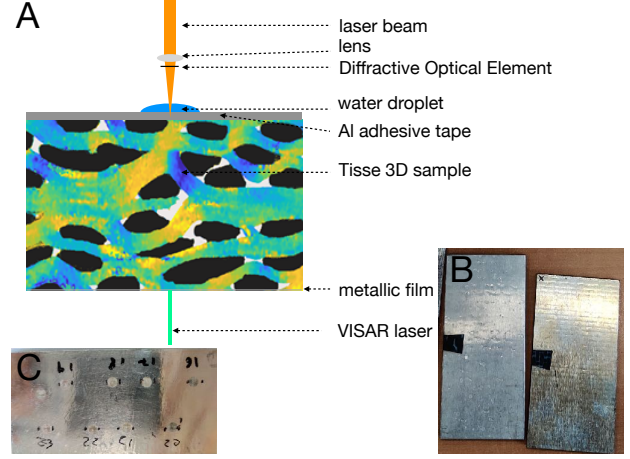

Figure 2. A: Scheme of the experimental set-up. B: Photography of the rear, silver-coated surface of two samples. C: Photography of the illuminated Al-adhesive layer after 8 shots.

Diffractive Optical Element (DOE), placed after the focusing lens, leads to an almost ideal top-hat spatial profile, almost perfectly circular with a homogeneous intensity profile (standard deviation of only 0.023) [4]. The top surface of the Tisse 3D target is covered by a thin (0.07 mm) aluminium adhesive tape, after surface cleaning with ethanol and removal of any possible fold with a plastic card. The intense laser beam ablates superficially this metallic layer over a thickness typically of 1.7-3 μm [5], sublimating it into a dense plasma. The droplet of water, a transparent dielectric material, confines the expansion and increases the surface pressure level imposed by the plasma expansion. As a result of the recoil moment of the ablated momentum, a pulsed shock wave is generated and propagates in the bulk of the Al layer. It is then transmitted into the Tisse 3D material. Sublimation of the aluminium layer and emission of a shock wave is a well-controlled and quantifiable process [4, 6]. The Al layer also protects the composite from the ablative laser impact, Fig.2.C. The lateral dimensions of the examined samples are approximately 45x90 mm^2. Two types of 3D woven composites were illuminated, with Type 2 having larger tows and a larger spatial period than Type 1. Three samples of thicknesses 2, 3 and 4.7 mm of Type 1 are illuminated, and two samples of thicknesses 3.7 and 7.5 mm of Type 2. For each sample, two series of four laser shots each, parallel to one another and aligned along one of the

main weaving axis, with shots and series separated by the distance of the quasi pattern, are performed (see the eight surface laser impacts on Fig.2.C). However, the number of successful shots per sample is variable, ranging between 3 and 8 (Tab.2). The laser intensity is adjusted for each sample in order to obtain similar velocity peaks measured at opposite surface for all samples, in the range 100-200 m/s, so as to make the comparison easier and to compensate for increased amplitude losses for the thicker samples. We select the laser fluency listed in Tab.2 by shooting on the sample a first time, measuring the amplitude, and then adjusting the fluency to maintain the desired velocity amplitude. Note that a previous study [4] shows that such type of bulk wave *propagation* can be considered as linear in metals (aluminum and titanium), even though the process of shock *emission* is highly nonlinear. As the present composite material is much more absorbing, we can expect this linear behavior to be even better satisfied here.

The surface velocity of the opposite surface is measured by VISAR laser interferometry. To obtain the required optical reflective surface at the VISAR laser wavelength (532 nm), an ultra-thin silver layer ($\sim$ 100 nm) is deposited by plasma deposition using an Electron Beam Evaporator PVD4-EB, Fig.2.B. The thickness of the silver layer being much smaller that the shock wavelength, 50 μm, this one does not exert any traction in the coating: at the shock wavelength, the deposit layer is indistinguishable from the free surface where the mechanical stress vanishes. In Fig.2.B due to its very small thickness, the silver layer is not able to cover all the micro-holes present over the composite surface, so that the metallized surface is not completely smooth. This however does not create any problem as the VISAR system is calibrated before every shot.

5. FDTD NUMERICAL METHOD

Among finite differences time domain (FDTD) methods, Virieux scheme [7] has proven to be highly efficient to simulate laser shock propagation in homogeneous and isotropic materials such as metals [4]. However, for general anisotropic materials, Virieux scheme cannot be applied straightforwardly because the grid staggering is not adapted anymore. We here use Lebedev schemes [8, 9] also using a grid staggering both in time and in space and locating all discrete velocities (noted generically W) on the same points of a first grid, and all stress components (noted generically S) on the same points of a second grid, staggered relatively to the velocity one by half

Sample	1	2	3	4	5
Thickness	2	3	4.7	3.7	7.5
Type	1	1	1	2	2
Fluency	7.3	13.5	16.43	16.21	20
Shots	3	8	5	8	5
Rise time	46	44	100	106	128
Rise time	52	98	157	96	143

Table 2. Main experimental parameters for each sample. Shots is the number of successful shots. For shock rise time, first line is measured one, second line is simulated one. Units are mm for thicknesses, J/cm^2 for fluencies, ns for rise times.

the spatial mesh $\Delta x/2$ in all directions. We can therefore note discrete spatial points ($x_i = i\Delta x/2, z_j = j\Delta x/2$) with (i, j) taking even values for velocity and odd ones for stress. Time grids are also staggered, with velocities computed at times $t_n = n\Delta t$ and stresses at times $t_n = (n + 1/2)\Delta t$. Spatial derivatives associated to one type of variable are computed by a fourth order, centered, finite difference

$$\left(\frac{\partial W}{\partial x}\right)^n_{i,j} = D_x(W^n_i) + O(\Delta x^4) \qquad (6)$$

$$\left(\frac{\partial S}{\partial x}\right)^{n+1/2}_{i,j} = D_x(S^{n+1/2}_i) + O(\Delta x^4) \qquad (7)$$

with

$$D_x(A^n_i) = \frac{27(A^n_{i+1,j} - A^n_{i-1,j}) - (A^n_{i+3,j} - A^n_{i-3,j})}{24\Delta x} \qquad (8)$$

and with odd (i, j) values for Eq.(6) and even ones for Eq.(7). Derivatives in the z-direction are obtained by the same finite difference scheme with differences in j-index instead of i-one. Time derivatives are evaluated by a second order, centered finite difference

$$\left(\frac{\partial S}{\partial t}\right)^n_{i,j} = \frac{S^{n+1/2}_{i,j} - S^{n-1/2}_{i,j}}{\Delta t} + O(\Delta t^2) \qquad (9)$$

$$\left(\frac{\partial W}{\partial t}\right)^{n+1/2}_{i,j} = \frac{W^{n+1}_{i,j} - W^n_{i,j}}{\Delta t} + O(\Delta t^2). \qquad (10)$$

Time and spatial steps are linked by the value of CFL=0.33 (computed on the highest sound velocity 13000

10th Convention of the European Acoustics Association
Turin, Italy 11th 15th September 2023 Politecnico di Torino
2898

m/s in the axial direction of fibers) ensuring stability. The mesh size Δx is chosen equal to four image pixel sizes (about 8 μm) instead of one, corresponding to about one sixth of the signal wavelength, which is satisfying for a fourth-order scheme in space. This results into a time step Δt of 0.2 ns. For initial conditions, we assume laser illumination starts only at initial time $t_i > \Delta t/2$, so that all velocity components are set to zero at time step $n = 0$, and all stress components at time step $n = 1/2$. For a simulation capturing three successive arrivals of the shock front at the rear surface of a 2-mm thick sample, the computation time on a laptop with an i5-6300HQ CPU at 2.30 GHz is approximately 45 minutes. For boundary conditions, we assume a known normal stress $\sigma_{xz}(x, z = 0, t) = 0$ and $\sigma_{zz}^{in}(x, z = 0, t) = f(t)H(x)$ on the illuminated surface. Thanks to the top-hat profile of the DOE, the spatial distribution of the laser stress is equal to 1 on the surface of the laser focal spot, 0 elsewhere. The pressure time waveform $f(t)$ results from the 1D ESTHER numerical simulation [10] of the deposition of laser energy (given by fluency from Tab.(2)) and of the evolution of the state of the illuminated aluminum surface layer from solid to plasma, taking into account radiative transfer and heat conduction. Mechanical models reproduce elasto-plasticity of the aluminum layer up to damaging and fracturation. This model is quantitative with no adjustable parameter, and has been proved efficient to model with high precision the input surface stress resulting from laser ablation for shock wave propagation in both aluminum and titanium [4]. We apply the resulting function time waveform $f(t)$ computed for aluminum directly on the composite surface, thus neglecting the influence of the aluminum thickness, its impedance mismatch with composite and its potential imperfect adhesion. Lateral boundaries, are sufficiently distant, and absorption of coherent signal due to scattering by the complex structure of the material is sufficiently high, so that their influence is negligible. The resulting algorithm has been validated by comparison with outputs of Virieux scheme applied to laser shock wave generated in aluminium [4], with perfect agreement between the two methods.

6. RESULTS

Analysis of experimental data and their comparison with simulations are performed from a statistical point of view because (i) detailed material geometry varies from sample to sample, and for a given sample, from shooting point to shooting point, (ii) 2D cuts used as geometrical inputs of simulations do not fully reflect the 3D actual local material structure beneath each shooting point. Therefore, for each sample thickness, we compare the VISAR measured velocities at the opposite free surface for the number of successful laser shots reported in Tab.(2), to the simulations performed using the eight local geometries extracted below the eight planed shots. We present results only for samples 2 (Type 1, thickness 3 mm) and 4 (Type 2, thickness 3.7 mm), which are the only ones with 8 successful shots. For both simulations (in red) and measurement (in blue), we report on Figs.(3-4) the mean value of the temporal velocity waveform, and the 95% probability computed by assuming a Student's t-distribution [11] as usual for samples of small size. To be able to perform statistics and compare the data, the velocity waveforms have been normalised in time so that the first shock always arrives at about unit dimensionless time 1. The reference time is, for each sample, the average of the measured first shock times of arrival. A comparison of the mean value and variability of the corresponding shock speed is presented on Fig.(5). For simulated signals, amplitudes have been adjusted manually to allow a statistical comparison. VISAR has a spatial resolution of 100 μm and a temporal one of 3 ns. For a spatial grid size Δx of about 8μm, this means we need to average the values of the velocity over 13 spatial grid points, and over 15 temporal ones. However, because of the "pixelization" of various boundaries within the samples and because of noise in the local orientation of the tows, the outputs of the FDTD simulations are quite noisy, even after this averaging. No particular handling of the detailed, complex geometries of the multiple interfaces within the Tisse3D has been tempted, so each simulation is smoothed spatially over 100 spatial grid points (but still over only 15 temporal ones) to reach a noise level similar to the measured one.

Figs.(3-4) show that, despite the complex structure of the material that is likely to induce multiple scattering, sharp wavefronts are still observable after the shock has travelled over one sample thickness, whatever this one. Multiple scattering results into an attenuation measurable as a finite shock rise time (time needed for the velocity to go from 10% to 90% of the peak amplitude) increasing with sample thickness, as reported in Tab.(2). Also clearly observable is the amplitude decay of the second arrival (at around dimensionless times 3) relatively to the first one, which is well predicted by simulations. Obviously, this arrival does not appear anymore as a sharp shock, contrarily to what is seen in homogeneous metals [4]. As no intrinsic absorption has been introduced in the model, this means
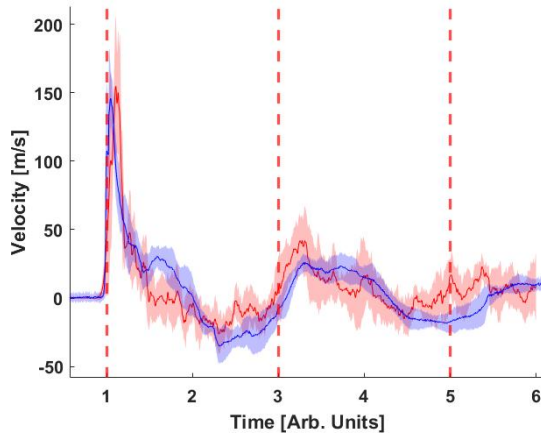
Figure 3. Mean value (thick line) and 95% probability (colored areas) of VISAR measurement (in blue) and FDTD simulations (in red) of measured opposite free surface velocity for sample 2 (type 1, thickness 3 mm). Times of arrival are normalised by mean experimental value. Amplitudes of simulations are adjusted to fit measured ones.

Figure 4. Same as Fig.3 for sample 4 (type 2, thickness 3.7 mm)

that structural attenuation simply by scattering of waves at the different material heterogeneities explains most of the overall attenuation. This is an important result, pointing out that only linear elastic parameters of the Tisse3D material are needed to predict most of its behaviour under LASAT exposure. However, when comparing measured and simulated rise times of Tab.(2), one can see that simulated ones tend to be shorter than measured ones. This difference cannot be due to the measurement system, as VISAR has a time resolution ten times less than the shortest measured rise time, and is spatially averaged over a smaller area than simulations. The most likely explanation is therefore physical absorption (potentially associated to dispersion), that influences only highest frequencies carried out by the shock. Third arrivals can also be distinguished for the 3 mm sample. Intermediate arrivals tend to be observed experimentally, possibly emanating from the edge of the focal spot. Such edge arrivals cannot be predicted at 2D [4] and indeed are not visible on simulations. Experimental variability of velocity waveforms seem moderate for thicknesses 3 and 3.7 mm, for which we have the largest number of data (8). It increases somewhat for other samples (not shown here) with a lower number of successful shots (3 or 5). For simulations, vari-
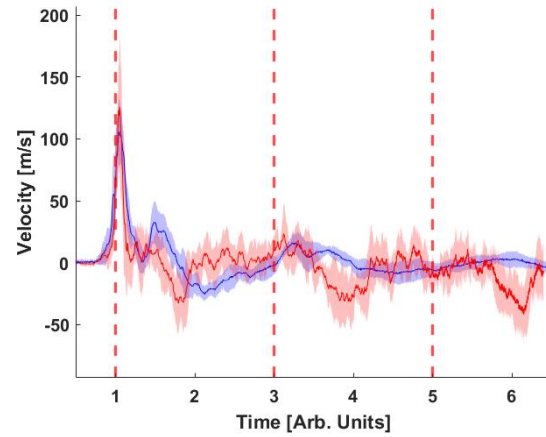
ability of results (always for 8 realizations) is smaller than the experimental one for the thinnest case, comparable for the 3 mm case, and tend to be larger for thicker samples. Once again, this may be due to the influence of the noisy model input data, that tend to increase simulation noise all the more as propagation distance increases.

Fig.(5) compares the measured and simulated mean velocities (along with its 95% probability) of shock first arrival, normalized by the mean value c_{mean} of all 29 experimental data. For Figs.(3-5), the time of arrival is defined as the first instant when the opposite surface velocity is equal to half (50%) the peak of the signal. Considering all samples and all 29 experimental values, variations of shock wave velocity are within an overall $\pm 4\%$ around reference. For a given sample, variations of shock wave velocity are within an overall $\pm 2\%$ range. Simulated values are systematically lower than measured ones, with also higher variability especially for the thinnest sample. The too low values of simulations can be explained by the 2D approximation. Indeed, in the 2D simulations, the Tisse3D is made of three different types of constituents: epoxy with a proportion α_e, tows orthogonal to the (xz) plane with a proportion α_t and in-plane tows with a proportion α_p. As the shock wave is clearly the first signal to arrive, we assume it propagates in each component material only with the highest wave speed within this component: otherwise, a signal would arrive before the shock, which is not what is observed. In epoxy (an isotropic material), the highest speed c_E is the one of longitudi-

nal waves. In orthogonal fibers (isotropic in their transverse section), the highest speed is the speed c_L of longitudinal waves in the transverse section. In in-plane fibers, the highest speed is c_F, that will be determined later on. Therefore, the highest possible speed in the z-direction is:

$$c_{2D} = \frac{1}{\dfrac{\alpha_e}{c_E} + \dfrac{\alpha_t}{c_l} + \dfrac{\alpha_p}{c_F}}. \qquad (11)$$

At 3D model, there is no reason to differentiate between in-plane and orthogonal fibers, both are equivalent, mainly orientated along the two weaving directions x and y and perpendicular to the wave propagation through the sample thickness z. The shock velocity is therefore given by the same Eq.(11) with $c_l = c_F$. The speed c_F can be estimated by searching for waves propagating in the z-direction:

$$(U, V) = (U_0, V_0)f(t - z/c_F) \qquad (12)$$

and similar notations for stress. Replacing Eq.(13) in the motion equations and eliminating stress, we get:

$$\begin{aligned}(\rho c_F^2 - c_{55})U_0 - c_{35}V_0 &= 0 \\ -c_{35}U_0 + (\rho c_F^2 - c_{33})V_0 &= 0. \end{aligned} \qquad (13)$$

It has a non-zero solution provided

$$(\rho c_F^2 - c_{33})(\rho c_F^2 - c_{55}) - c_{35}^2 = 0 \qquad (14)$$

which has two solutions:

$$c_F = \sqrt{\frac{c_{33} + c_{55} \pm \sqrt{(c_{55} - c_{33})^2 + 4c_{35}^2}}{2\rho}}, \qquad (15)$$

the one with the "+" sign being the sought after, fastest one c_F. In the particular case of fibers parallel to the x-direction, $\theta = 0$ and $c_{35} = 0$. According to data $c_{55} > c_{33}$ and the fastest wave is $c_{F0} = \sqrt{c_{55}/\rho}$ with $V_0 = 0$: the F (for "fast") wave is a transverse wave polarized in the horizontal x-direction perpendicular to the propagation one. In case fibers are not perfectly horizontally orientated, c_F gets larger than c_{F0} because of the contribution of c_{35}. Note a fast transverse wave is here possible because we have not considered waves propagating in the x-direction at speed $\sqrt{c_{11}/\rho}$ which is much larger.

According to the various data collected from the analysis of sample images, we found a mean proportion of 7% of epoxy, 40% of transverse fibers and 53% of in-plane fibers. The mean value of the orientation angle is around 10°. Using this mean angle to compute c_F, one can evaluate the shock wave velocity according to the 2D and 3D models. Renormalizing it by c_{mean}, one obtains $c_{2D}/c_{mean} = 0.961$ and $c_{3D}/c_{mean} = 1.015$. They differ by about 7.5%. Both values are reported on Fig.(5). The 3D value is slightly above the mean of experimental data (+1.5%), and within error bars for the most reliable (8 shots) 3 and 3.7 mm cases. The 2D value is somewhat lower, following the trend observed for simulations but being nevertheless higher than the average of simulations. It is also within the error bars for all samples except the 2 mm case. For this case, one particular sample has an epoxy spot much larger than the average, which tends to decrease the overall homogenized sound speed. However the difference between the 2D and 3D models is not so large, and numerous parameters (material stiffnesses, proportion of epoxy within the tows, proportion of various components, rotation angle of tows...) have a degree of variability that may also explain the observations.
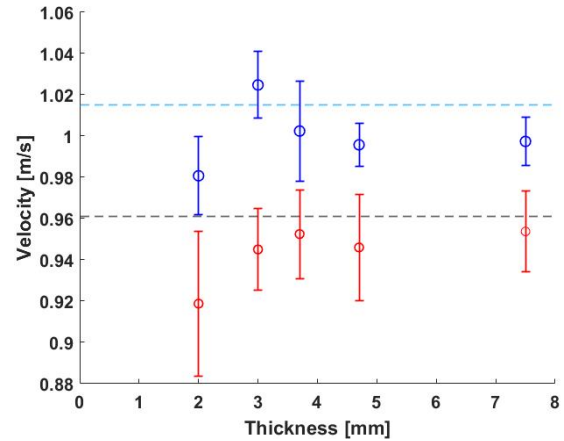

Figure 5. normalized velocity of the first shock-wave versus sample thickness. Comparison between experiments (in blue) and simulations (in red), with mean value (circles) and 95% probability (error bars). Lower (resp. upper) dashed line is 2D (resp. 3D) homogenization model.

7. CONCLUSION

This paper investigates the propagation of a laser shock wave within a composite material used in aeronautics and made of carbon fibres woven according to a 3D pattern

within an epoxy matrix. The shock wave is generated by an impulsive intense laser beam focused on the surface of a thin metallic layer attached to the composite. A measurement campaign has been performed for five different samples and eight shots for each sample. A 2D numerical model has been developed based on a FDTD discretisation of the equations of linear elastodynamics for the propagation part, combined with a nonlinear model of the source. Sample plane geometry and in-plane fibres orientations are obtained from analysis of the images of transversal cuts of the samples. Experimental data are statistically compared to the model and discussed. A clear, sharp shock wave is observed for the first arrival, with rise time increasing with sample thickness. Second arrival after traveling through three sample thicknesses is strongly smeared out by ultrasound attenuation. This one is dominated by geometrical scattering at the multiple inner material interfaces, as indicated by the good agreement between simulations and experiments. The velocity of the first shock arrival shows some small variability, and 2D simulations tend to underestimate it compared to 3D observations. Simulated amplitudes are not discussed here as they are difficult to predict due to the presence of the illuminated thin, metallic layer. This one should be taken into account in the future, along with 3D effects.

8. REFERENCES

[1] J. Schindelin, I. Arganda-Carreras, E. Frise, V. Kaynig, M. Longair, T. Pietzsch, S. Preibisch, C. Rueden, S. Saalfeld, B. Schmid, J.-Y. Tinevez, D. J. White, V. Hartenstein, K. W. Eliceiri, P. Tomançak, and A. Cardona, "Fiji: an open-source platform for biological-image analysis," *Nature Methods*, vol. 9, no. 7, pp. 676–682, 2012.

[2] M. Abramoff, P. Magalhães, and S. Ram, "Image processing with ImageJ," *Biophotonics International*, vol. 11, pp. 36–42, 2003.

[3] Z. Puspoki, M. Storath, D. Sage, and M. Unser, "Transforms and operators for directional bioimage analysis: A survey," in *Focus on Bio-Image Informatics*, pp. 69–93, Springer, 2016.

[4] E. Cuenca, M. Ducousso, A. Rondepierre, L. Videau, N. Cuvillier, L. Berthe, and F. Coulouvrat, "Propagation of laser-generated shock waves in metals: 3D axisymmetric simulations compared to experiments," *Journal of Applied Physics*, vol. 128, no. 24, pp. 244903 (1–13), 2020.

[5] M. Scius-Bertrand, L. Videau, A. Rondepierre, E. Lescoute, Y. Rouchausse, J. Kaufman, D. Rostohar, J. Brajer, and L. Berthe, "Laser induced plasma characterization in direct and water confined regimes: new advances in experimental studies and numerical modelling," *Journal of Physics D: Applied Physics*, vol. 54, no. 5, pp. 055204 (1–14), 2020.

[6] S. Bardy, B. Aubert, L. Berthe, P. Combis, D. Hébert, E. Lescoute, J.-L. Rullier, and L. Videau, "Numerical study of laser ablation on aluminum for shock-wave applications: development of a suitable model by comparison with recent experiments," *Optical Engineering*, vol. 56, no. 1, pp. 1–8, 2016.

[7] J. Virieux, "SH-wave propagation in heterogeneous media: Velocity-stress finite-difference method," *Geophysics*, vol. 49, no. 11, pp. 1933–1942, 1984.

[8] V. I. Lebedev, "Difference analogues of orthogonal decompositions, basic differential operators and some boundary problems of mathematical physics. I," *USSR Computational Mathematics and Mathematical Physics*, vol. 4, no. 3, pp. 69–92, 1964.

[9] V. Lisitsa and D. Vishnevskiy, "Lebedev scheme for the numerical simulation of wave propagation in 3D anisotropic elasticity," *Geophysical Prospecting*, vol. 58, no. 4, pp. 619–635, 2010.

[10] J.-P. Colombier, P. Combis, F. Bonneau, R. Le Harzic, and E. Audouard, "Hydrodynamic simulations of metal ablation by femtosecond laser irradiation," *Physical Review B: Condensed Matter and Materials Physics*, vol. 71, pp. 165406 (1–6), 2005.

[11] G. B. Arfken, H. J. Weber, and F. E. Harris, "Probability and statistics (ch. 23)," in *Mathematical Methods for Physicists*, pp. 1125–1179, Academic Press, 2013.

9. ACKNOWLEDGMENTS